2023 IEEE/ASME International Conference on
Advanced Intelligent Mechatronics (AIM)

Force control of a grinding robotic manipulator with floating base via model prediction optimization control

Changkook Seo[1], Hanbom Kim[1], Hongjoo Jin[1], Taegyun Kim[2], TaeWon Seo[1], *Senior Member, IEEE*

***Abstract*—In this paper, a grinding robot for large area and an impedance-based force control method applied to the robot are described. With the development of science and technology, the demand for various industrial robots increased, and among them, the demand and importance of grinding robots that require high risk and precision increased. In particular, research on grinding robots targeting large areas has not been conducted relatively, and accordingly, the design and control mechanism of robots specialized in large areas was needed. A robot consisting of a manipulator and a grinding module with a 2-DoF parallel structure is proposed as the design of a new grinding robot. The control method is based on impedance force control mainly used in existing grinding robots, but to overcome the limitations of using only impedance control, the impedance control via model-based prediction optimize(MPO) is proposed as a control technique for grinding robots. Experiments were conducted to verify the force tracking ability of the proposed control, resulting in a 28.1% improvement in settling time for the desired force. Even for disturbance, more improved recovery performance than conventional controllers has been verified. As a result, proposed impedance force control via MPO shows improved force tracking performance over conventional impedance control, and is presented as one of the appropriate control methods for grinding robots targeting large areas.**

***Index Terms*—Grinding robot, Optimal impedance control, Model-based prediction control**

I. Introduction

The production of parts requiring more sophisticated and dangerous work has increased the demand for the industrial robot market to perform tasks on behalf of humans. In particular, interest in industrial robots has increased significantly in the grinding market [1]. In fact, according to the accident records of Construction and fabrication companies, the highest accident rate between 2015 and 2018 was an accident during grinding work, and the biggest cause was human error [2]. The need to introduce industrial robots in the grinding industry has been highlighted.

*This research was supported by Basic Science Research Program through the National Research Foundation of Korea(NRF) funded by the Ministry of Education(No. NRF-2021R1I1A3059727) (Corresponding authors: TaeWon Seo, Taegyun Kim)

Changkook Seo[1], Hanbom Kim[1], Hongjoo Jin[1], TaeWon Seo[1], are with the School of Mechanical Engineering, Hanynag University, Seoul 04763, Republic of Korea sck950525@gmail.com, hopebom77@gmail.com, joha123@hanyang.ac.kr, taewonseo@hanyang.ac.kr

Taegyun Kim[2] is with Mechanical Engineering, Yeungnam University, Gyeongsan 38641, Republic of Korea tgkim@yu.ac.kr

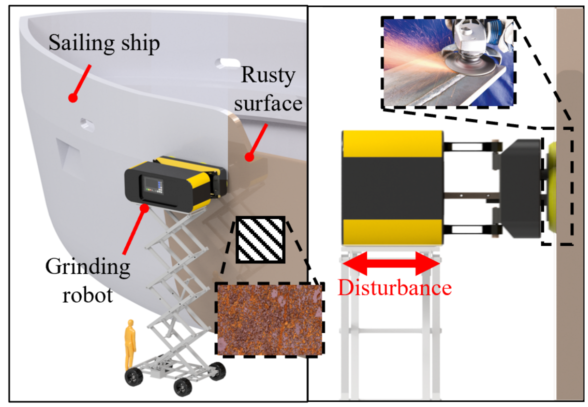

Fig. 1. Proposed large area grinding robot.

Many developments and studies have been conducted on grinding robots; However, most of the results were focused on grinding small, sophisticated parts. Demand for grinding work on large areas, such as ship and tank parts, was still performed by humans [3], [4]. Large-area grinding workers were still taking safety risks. Large scale grinding is still highly labor intensive. [5] Existing grinding robots use fixed manipulator arms [6]. The work is carried out after fixing the grinding object to the fixed workstation [7]. This structure and work method are not suitable for performing grinding work on a large area of a large target such as ship parts or military parts. To address this, a new grinding robot was developed, which has a structure that contacts the grinding module and the target through a mobile platform-based floating base and a two-degree manipulator. Furthermore this mechanism is MIMO nonlinear system with 2 input and 2 output, where manipulator of a robot rotates 2 links to control the position and angle of the grinding module [8].

Most grinding robots use the impedance control proposed by Neville Hogan as a force control method [9]. Impedance control was mainly used in contact situations with the manipulator robot and environment, and is a method used with integrated controllers implementing compliant elements [10], [11]. The purpose of impedance control is to establish a desired dynamic relationship with a mass-spring-damping system between posture and contact force, which is usually referred to as the target impedance [12]. The impedance controller includes a torque-based impedance control and a position-based impedance control, among which a position-based impedance control is called an admittance control [13]. Admittance control has advantages when the characteristics of the actual manipulator are not well known or when it is difficult to predict the torque required for movement, which is suitable for use in designed grinding robots [14]–[16]. Impedance control provides a way for designers to control the manipulator to interact with its surroundings in the desired form [17], [18]. By adjusting the impedance characteristics represented by Mass, spring, and damper, the desired manipulator movement is created, and it has some robustness against modeling errors in the surrounding environment [19]–[21]. In addition, impedance control allows natural movement in both situations where the robot is in contact with or out of contact with the surface [10].

There are some limitations on controlling the grinding robots using the impedance control solely. Since large outer force including high amplitude vibration is generated during the grinding process and the applied force should be large enough to make the abrasive to contact on the target surface more firmly, control for larger force is necessary. Therefore, to compensate for this, impedance controls combined with various means such as adaptive impedance control [22], [23], fuzzy impedance control [24], and other intelligent impedance control [25] have been studied as actual grinding contact force control methods [26]. However, in order to perform large-area grinding tasks, it is essential to prevent damage to the grinding surface and robot caused by the excessive reaction force while also minimizing the settling time for efficient operation. Existing adaptive impedance control methods have the disadvantage of slow convergence speed when the difference between the Desired Stiffness and the Actual stiffness of the work surface is large. Additionally, fuzzy impedance control requires tuning parameters for each case, which involves many decision variables and makes optimization difficult. As explained above, mobility for the robot is necessary in case of large scale grinding where target surface is larger than the grinding robot itself. Therefore causing extra external force from the movement of the robot and calculation of reaction force from it to keep the proper exerting force. For the distance between the robot and the target surface as the robot moves, more rapid impedance gain control is also needed.

In this paper, impedance control via model-based prediction optimize is proposed as a new control method for grinding robots for large area grinding tasks. There are limitations in controlling the impedance control alone in a grinding environment where the robot is not fixed and is based on a floating base, and there are many disturbances such as vibration. Based on the dynamic model, the impedance control is reinforced by adjusting the coefficient of impedance control through an optimization technique using the predicted model. Based on these ideas, finally model prediction-based impedance force control is proposed as a robust controller against disturbances.

This paper consists of five sections. Section 2 describe the robot mechanism. Section 3 include the contents of control of robot. Section 4 show the experiment set up and result of experiment and Section 5 is conclusion of paper.

II. Robot configuration

In this section, the proposed grinding robot is described. After the overall structure is explained, the grinding module and the 2-DOF manipulator are mainly described.

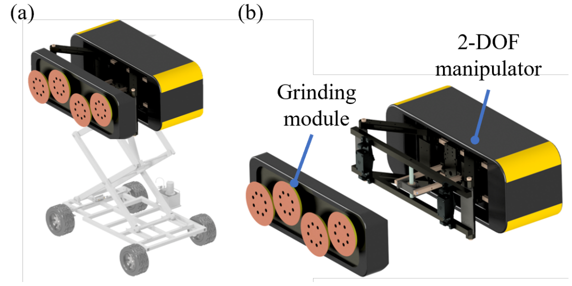

Fig. 2. Overall design of proposed grinding robot. (a) The robot positioned on a mobile platform, and (b) components of grinding robot.

A. Overall structure

Fig. 2 represents the overall design of the robot proposed for large-area grinding. The robot is largely composed of three components: a grinding module, a two-degree freedom manipulator, and a mobile platform. Grinding work begins while approaching the grinding target through the mobile platform. When approaching the object at a certain distance or less, the grinding module is brought into contact with the object through a 2-DOF manipulator. The 2-DOF manipulator can perform impedance control through the function of spring and displacement measurement, which allows the grinding module to maintain contact with the target with a constant force. The grinding is performed through a sanding pad attached to the grinding module, and a large area is processed at once through surface contact with the object. The grinding module has a structure that is easy to attach and detach from the manipulator, so it is easy to assemble, and the grinding pad can be replaced in consideration of the diversity of the surface of the object.

B. Grinding module

As shown in Fig. 2, the grinding module grinds the target through a total of four grinding pads. The four pads are rotated by two motors through the gear train construction. A BLDC motor (Bevel planetary reduction gear BLDC motor BG42-BL4299 DC24V 105W, motorbank) was used, and a decelerator with a deceleration ratio of 1/14 was used to achieve a rated speed of 286 rpm and a rated torque of 2.835Nm. The grinding pad consists of a sanding pad that directly contacts the target and a backup pad that can be attached with sanding pad and has a damping effect. The sanding pad and the backup pad are combined in a velcro type, thereby facilitating replacement of the sanding pad according to the surface state of the grinding object. The grinding module has a size of 640 mm wide and 140 mm long, and the size of the grinding pad is 5 inch.

C. 2-DoF manipulator

The structure of the 2-DOF manipulator is shown in Fig. 3. The structure of the manipulator is based on the previously studied 2-DOF parallel structure [27]. The manipulator allows the grinding module to perform two degrees of freedom: forward and backward movement and rotation. Using the belt-pulley, the compliance structure is moved along the linear guide to allow the manipulator to take the desired action. Depending on the length of the manipulator arm, the maximum

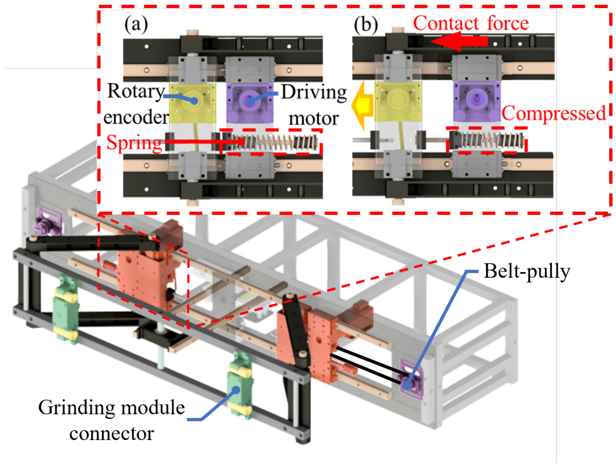

Fig. 3. Mechanism of 2-DOF manipulator. Red box above indicates the design of compliance structure. Principle of operation of compliance structure for contact forces.

(a) (b)

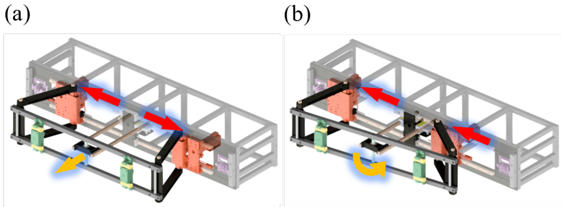

Fig. 4. Describe 2-DOF movement of manipulator.(a) Manipulator moving in linear motion. (b) Manipulator moving in angular motion.

travel range is 200 mm forward and the rotation is 10 degrees. In addition, the 2-DOF manipulator can perform impedance control by measuring the force applied to the robot through a compliance structure marked with a red dotted square as shown in Fig. 3. The compliance structure consists of a carriage equipped with an encoder sensor that measures the displacement of the spring relative to the spring and a carriage equipped with an actuator that moves the manipulator arm [28]. When the grinding robot contacts the object and a contact force is generated, the force is transmitted to the compliance structure through the manipulator arm. The carriage with the rotary encoder moves by the force transmitted as in Fig. 4 (b), thereby compressing the spring. It is possible to calculate the contact force between the grinding robot and the object through the known spring characteristics and the spring compressed distance value measured through the encoder. The calculated force data is used as the main data for robot impedance control.

III. Control System

In this section, the robot's control system, model prediction based impedance control, is described. The description of the robot's kinematic and dynamic is followed by the description of the robot's control system.

Nomenclature

ϕ	Rotation angle of grinding module [rad]
θ_1	Moving angle of the left linkage arm [rad]
θ_2	Moving angle of the right linkage arm [rad]
a	Distance from linkage end to module connector [mm]

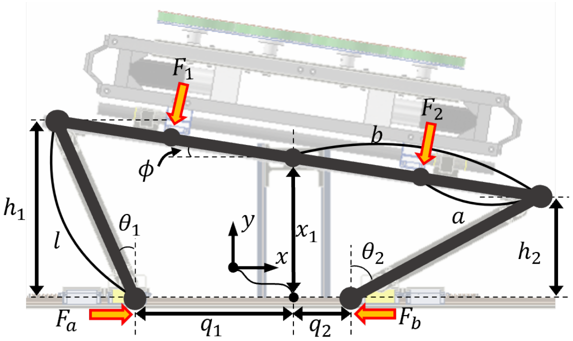

Fig. 5. Kinematic model for 2-DOF manipulator. The explanation of each symbols are presented above.

b	Half length of the grinding module [mm]
F_1	External force applied to left side of grinding module
F_2	External force applied to right side of grinding module
F_a	Left force applied to move the 2-DOF manipulator
F_b	Right force applied to move the 2-DOF manipulator
h_1	Left height between base and grinding module [mm]
h_2	Right height between base and grinding module [mm]
l	Length of linkage arm [mm]
m_1	Weight of left linkage arm [kg]
m_2	Weight of right linkage arm [kg]
m_e	Weight of grinding module linkage [kg]
q_1	Linear distance of the left driving motor [mm]
q_2	Linear distance of the right driving motor [mm]
x_1	Height of the 2-DOF manipulator linear motion [mm]

A. *Kinematics and Dynamics of grinding robot*

Fig. 5 shows the kinematic model of the 2-DOF manipulator.

The kinematic constraints obtained from kinematic modeling of the 2-DOF manipulator are:

$$\begin{aligned}(q_1 - b\cos\phi)^2 + (x_1 + b\sin\phi)^2) &= l^2 \\ (q_2 - b\cos\phi)^2 + (x_1 - b\sin\phi)^2) &= l^2\end{aligned} \tag{1}$$

Based on Eq. (1), the moving distances q_1 and q_2 of the manipulator driving motor are represented for the positions of ϕ and x_1 of the endpoints:

$$\begin{aligned}q_1 &= b\cos\phi - \sqrt{l^2 - (x_1 + b\sin\phi)^2)} \\ q_2 &= b\cos\phi - \sqrt{l^2 - (x_1 - b\sin\phi)^2)}\end{aligned} \tag{2}$$

The force of two points generated by the manipulator when the grinding module contacts the target is called F_1 and F_2, and the distance from the manipulator is defined as h_1 and h_2, respectively. At this time, h_1 and h_2 are expressed as,

$$\begin{aligned}h_1 &= x_1 + b\sin\phi \\ h_2 &= x_1 - b\sin\phi\end{aligned} \tag{3}$$

The forces F_a and F_b applied to the compliance of the manipulator are calculated through the spring of the compliance. The spring coefficient of the spring of compliance and the position information obtained from the rotary encoder attached to the compliance carriage are calculated, and the resulting force is obtained as follows,

$$F_a = k_s(x_k - x_a)$$
$$F_b = k_s(x_k - x_b) \tag{4}$$

Values k_s, x_k, x_a, and x_b refer to the spring coefficient, the initial length of the spring, and the changed length of the spring obtained from the rotary encoders, respectively. The spring coefficient k_s is a known number, and values of x_a and x_b are maintained through the linear encoder and the rotary encoder mounted on the manipulator.

The Jacobian equation is,

$$\begin{bmatrix}\dot{q_1}\\ \dot{q_2}\end{bmatrix} = J^{-1}\begin{bmatrix}\dot{h_1}\\ \dot{h_2}\end{bmatrix},\ J = J_q^{-1}J_xJ_h^{-1} \tag{5}$$

Where, $J_h = \begin{bmatrix}-1 & -b\cos\phi\\ -1 & b\cos\phi\end{bmatrix}$,

$J_q = \begin{bmatrix}q_1 - a\cos\phi & 0\\ 0 & q_2 - a\cos\phi\end{bmatrix}$,

$J_x = \begin{bmatrix}x_1 + a\sin\phi & q_1 a\sin\phi + x_1 a\cos\phi\\ x_1 - a\sin\phi & q_2 a\sin\phi - x_1 a\cos\phi\end{bmatrix}$

Differential progress is made for Eq. (1) and Eq. (3) to express the forces on F_1, F_2 that occur when the grinding module and the target come into contact as forces F_a, F_b applied. J_h can be obtained by differentiating Eq. (3). J_q is obtained by partial differentiation of Eq. (1) for q_1 and q_2, and J_x is obtained by partial differentiation for x_1 and ϕ, respectively. The details about this equations are referenced from this paper [13]. The relationship between the contact forces F_1 and F_2 through the Jacobian matrix obtained in (5) and the forces F_a and F_b measured in compliance is given in Eq. (6).

$$\begin{bmatrix}F_a\\ F_b\end{bmatrix} = J\begin{bmatrix}F_1\\ F_2\end{bmatrix} \tag{6}$$

In order to execute impedance control, information on the force of the grinding module to contact the object was required. Control over contact forces is possible through a relationship involving a Jacobian matrix between the contact force and the force measured through the compliance structure of the manipulator. As shown in Fig. 3, the compliance structure using springs prevents sensor noise generated when measured through load cells, enabling stronger control.

The dynamics of the grinding robot are calculated through the Lagrangian equation.

$$\frac{d}{dt}\left(\frac{\partial T}{\partial \dot{q}}\right) - \frac{\partial T}{\partial q} = F \tag{7}$$

Where, $q = \begin{bmatrix}q_1\\ q_2\end{bmatrix}$, $F = \begin{bmatrix}F_1 - F_{ext}\\ F_2 - F_{ext}\end{bmatrix}$

Assuming that the force in the direction of gravity is negligible, the Lagrangian equation by the manipulator sending the potential energy by gravity to zero. T is,

$$T = \frac{1}{2}mV_1^2 + \frac{1}{2}I_1\dot{\theta_1}^2 + \frac{1}{2}mV_2^2 + \frac{1}{2}I_2\dot{\theta_2}^2 + \frac{1}{2}I_3\dot{\phi}^2 + \frac{1}{2}m_eV_3^2 \tag{8}$$

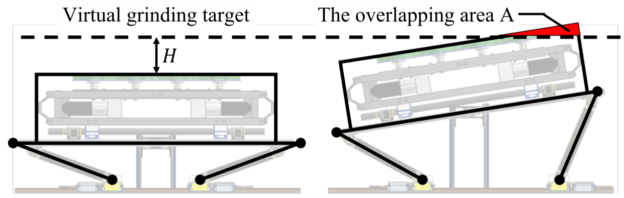

Fig. 6. Illustrative robot movement for calculation the reaction force between virtual target surface and the grinding robot.

As explained in Fig. 5, manipulator consists of two arm-bars corresponding to length l and an end-bar of length $2b$ that connects to the grinding module. The mass of the arm-bar is m and the sum of the mass of the end-bar and the mass of the grinding module is called m_e. The values V_1 and V_2 respectively mean the speed value of arm-bar, and V_3 means the end-bar speed value. These can be expressed with derivative of the angle and length.

$$V_1 = \frac{1}{2}\dot{\theta}_1,\quad V_2 = \frac{1}{2}\dot{\theta}_2,\quad V_3 = -lsin\theta_1\dot{\theta}_1 - bcos\phi\dot{\phi} \tag{9}$$

The value I represents the inertia value of each bar. Here, θ_1 and θ_2 can be expressed with q_1 and q_2 and following.

$$\theta_1 = \frac{\pi}{2} + \frac{(b-q_1)^3}{(6l^3)} + \frac{b-q_1}{l}$$
$$\theta_2 = \frac{\pi}{2} - \frac{(b-q_2)^3}{(6l^3)} - \frac{b-q_2}{l} \tag{10}$$

F_1 and F_2 are the force at the end by the manipulator expressed in Fig. 5. Further, obtained dynamics are finally expressed as Eq. (11).

$$M(q)\ddot{q} + V(\dot{q}, q) = F \tag{11}$$

$\ddot{q}$ is represented by equation (12) as follows:

$$\ddot{q} = M^{-1}(q)(F - V(\dot{q}, q)) \tag{12}$$

The dynamics allow us to calculate the location information $\ddot{q}$ of manipulator.

F_{ext} is an external force, which means a reaction force generated by a grinding object. The implementation of the force against the reaction force is achieved through modeling of the reaction force by creating a virtual grinding object. Assuming a situation in contact with a grinding object, the area generated by overlapping the manipulator is,

$$A = \frac{1}{2}\left(a\cos\phi - \frac{H - x_1}{\tan\phi}\right)(a\sin\phi + x_1 - H) \tag{13}$$

H is the distance between the grinding object and the manipulator. Thus, F_{ext} is represented by K_{ext}, which is the stiffness of the virtual grinding object.

$$F_{ext} = K_{ext}A \tag{14}$$

The value of K_{ext} was adjusted through repeated experiments comparing it with the motion of a real robot. $K_{ext} = 20000$ was set to have an error rate of about 1% with respect to the contact environment.

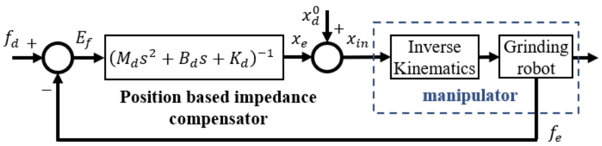

Fig. 7. Position based impedance control system

B. Position based impedance control

The position-based impedance control applied to the two-degree of freedom manipulator used in the grinding robot follows the form expressed in Fig. 7.
The equation for the target impedance is,

$$M_d \ddot{x}_{dc} + B_d \dot{x}_{dc} + K_d x_e = -E_f \tag{15}$$

where, M_d, B_d, and K_d are the desired mass, desired damping coefficients, and desired stiffness of the controller, respectively. x_d refers to the desired position of manipulator and x_c is the compliant position value of manipulator and position correction between x_d and x_c is $x_e = x_d - x_c$. f_d refers to the desired force and f_e refers to the actual contact force of the robot obtained through compliance structure and $E_f = f_d - f_e$. The forces above is relevant to the external forces F_1 and F_2 in Fig. 5. The force of the spring of the compliance structure described above is used to calculate the actual contact force applied to the robot. Through impedance control, contact force and moment are controlled at the end-effector end of the 2-dof manipulator which is in contact with the target during grinding.

Through impedance control, desired force gives an input in the form of a step function. However, the distance between the wall and the robot represents a continuous functional form and the performance deteriorates because the dynamic relationship between the real wall and the manipulator of the grinding robot is not fully considered. To compensate for these limitations, the compensation coefficient η is established and the desired position x_d value is expressed by Eq. (16). The value x_d is equal to the resulting input value x_{in} of Fig. 7.

$$x_d = x_d^0 + \eta x_e \tag{16}$$

Accordingly, the first-order differential and second-order differential values of x_e follow the following equation.

$$\dot{x}_e = \frac{\dot{x}_c}{\eta - 1}, \quad \ddot{x}_e = \frac{\ddot{x}_c}{\eta - 1} \tag{17}$$

C. Impedance control via model-based prediction optimize

A model-based prediction optimization(MPO) method is used as a method to enhance impedance control. Model-based prediction optimization is a strategy to optimize by predicting a finite horizon based on information on the initial state and information on the current state of the system by solving the dynamic model of the robot [29], [30]. Fig. 8 describes the entire control system to which this method is applied.

The main purpose of robot force control is to minimize the E_f value, the difference between the desired force f_d and f_c. The E_f value is predicted through a dynamic model and a control algorithm. The prediction process proceeds for N^{th} finite loop intervals. Cost function is determined through the predicted future error value and optimization is carried out to update the K_d value, which is the stiffness value of the impedance compensator, to strengthen the existing impedance control. The control algorithm is created by Eq. (15) and Eq. (16) and is expressed as,

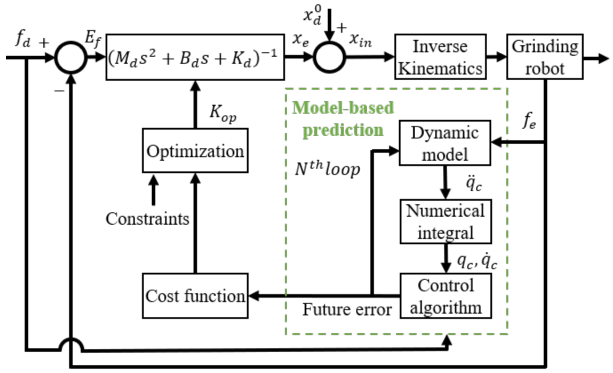

Fig. 8. Block diagram of control system

$$-E_f = M_d\left(\frac{\ddot{x}_c}{\eta - 1}\right) + B_d\left(\frac{\dot{x}_c}{\eta - 1}\right) + K_d\left(\frac{x_c}{\eta - 1}\right) \tag{18}$$

The dynamic model allows us to obtain values of x_c, $\dot{x}_c$, $\ddot{x}_c$, and the values of mass and damping coefficients of the impedance compensator, M_d and B_d, give constant values for the system. As a result, E_f is represented by an expression for K_d. The cost function to be minimized include a force tracking error, $E_f = f_d - f_e$.

From Eq. (18), the position control input of the controller can be calculated, and the reaction force f_e can be predicted by substituting it into Eq. (11). Each equation calculated E_f in each step through z-transform, and the cost function is as shown in Eq. (19).

$$J_{cost} = \sum_{i=k}^{k+N} [E_f(i)^T E_f(i)] \tag{19}$$

The value k is the time instant and N is the size of the prediction horizon. As mentioned earlier, it is assumed that the parameters M_d and B_d for mass and damping on the system are constant. Finally, the cost function J_{cost} is represented by an expression for K_d, which is a impedance parameter. As a result, it becomes a problem to find a K_d value that minimizes the cost function and is defined as follows:

$$\min_{\mathrm{K_d(k)}} J_{cost} \tag{20}$$

where, $K_d^{min} \leq K_d(k) \leq K_d^{max}$. The K_d^{min} was determined through stability analysis as follows.

$$E_f = f_d - f_e = f_d - K_{ext}(x_c - x_e) \tag{21}$$

To sum up the above equation,

$$x_c = x_e + \frac{f_d - E_f}{K_{ext}} \tag{22}$$

Here, substitute Eq. (22) for Eq. (18) and organize expression

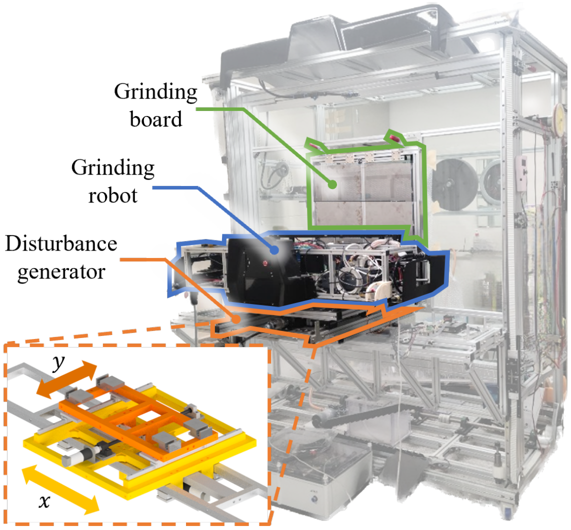

Fig. 9. Design of testbench

for $E_f(s)$ through Laplace transform.(where, $f_d = const$)

$$\mathscr{L}\left(E_f(t)\right) = E_f(s), \quad \mathscr{L}\left(x_e(t)\right) = X_e(s) \tag{23}$$

$$E_f(s) = \frac{k_e(M_d s^3 + B_d s^2 + k_d s)X_e(s) + k_d f_d}{M_d s^3 + B_d s^2 + (k_d - K_e xt + K_{ext})s} \tag{24}$$

If the curvature of the wall is large, the distance changes slowly. Therefore x_e can be assumed as a step input, and $(k_d - K_{ext}\eta + K_{ext}) > 0$ must be satisfied in order for the Eq. (24) to be stable. In addition, the value of K_d changed rapidly due to the problem that the reaction force was not measured while the grinding unit approached the wall in Free Space, and the system became unstable due to the motor's saturation. Thus K_d^{max} decided experimentally.

The equation of optimization becomes a problem of minimizing $J_{cost}(K_d(k))$. QP solver is used as a tool to solve the optimization problem.

IV. Experiment Result

A. Lab test-bench

Verification of the model prediction-based force control system was performed through lab experiments. The design of the test bench manufactured in consideration of the situation of disturbance by the mobile platform is the same as that of Fig. 9. The test bench consists largely of a grinding board that will hold the iron plate to be ground, a mobile platform, and a disturbance generator that will implement other disturbances. The grinding board is equipped with six plates that will be the target of the grinding work. A 1.5T thick steel plate with a size of 310mm x 200mm was used as the target plate for the grinding work used in the experiment. The grinding robot has a structure that can be attached to the disturbance generator, and is configured to move by the disturbance generator. The disturbance generator is manufactured to realize a desired disturbance and the structure is shown in detail in Fig. 9.

B. Application of impedance control via MPO

The impedance control via model-based prediction optimization(MPO) was applied to the control system of grinding robot. Experiments were conducted through an actual robot to confirm the performance of the new control method. The grinding robot's controller hardware uses CompactRIO (National Instrument cRIO-9024) equipped with NI-DAQmx. The sampling time of the controller is set to $10ms$ and operates. The initial set value of the impedance control used in the experiment was the previously used impedance coefficient value (M_d = 1, B_d = 20, K_{d_0}= 1000). First, it was applied to the manipulator itself without considering the disturbance of grinding, and the result can be seen in Fig. 10 (a). Preliminary experiments confirmed that more than 10N was required for polishing, and there was no significant difference in polishing performance at reaction forces beyond that. However, we set the target force to 20N because too high reaction force can affect the durability of the robot. It also aimed to minimize overshoot and setting time at the same time through MPO's cost function. For the number of model prediction loops used for optimization, experiments were conducted up to the number of loops N = 30 and compared. It can be seen that as the number of loops increases, the performance improves to have a faster settling time for the desired force. When setting the number of loops N to 30, an increase in the computational workload required for optimization is observed, resulting in fluctuations in the sampling time between 10ms and 11ms. By comparing the number of inputs obtained through optimization, the system achieved steady state at the 354th input

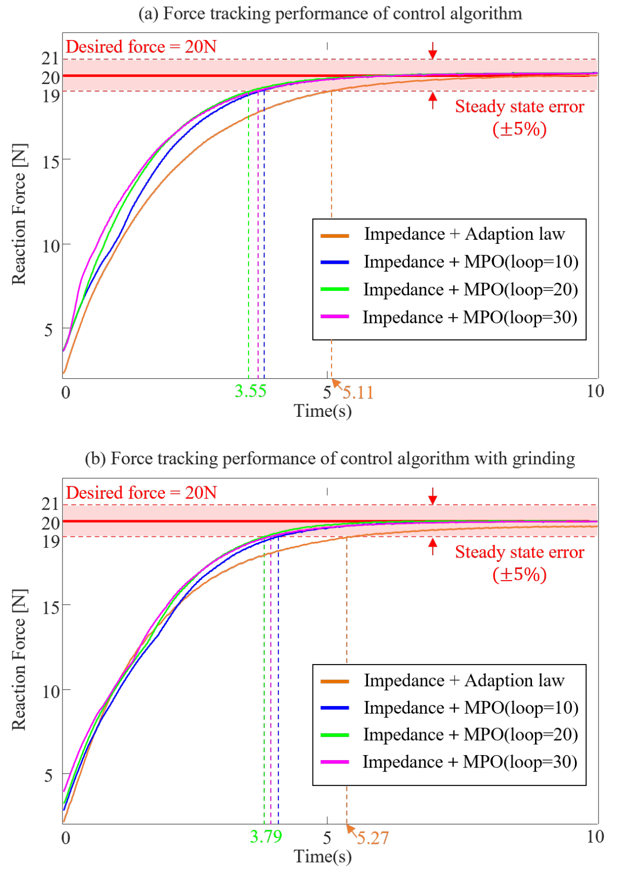

Fig. 10. Force tracking performance of control algorithm. (a) Force tracking performance without grinding. (b) Force tracking performance with grinding (N is number of prediction loops)

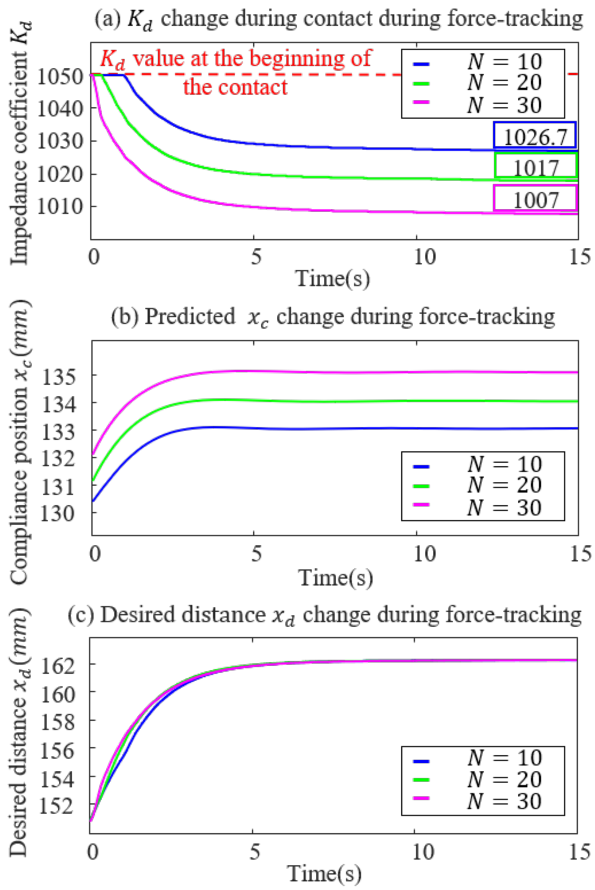

Fig. 11. Changes in control algorithm's key values during force-tracking. (a) Impedance coefficient K_d changes during force-tracking. (b) Predicted x_c changes during force-tracking (c) Desired distance x_d changes during force-tracking (N is number of prediction loops)

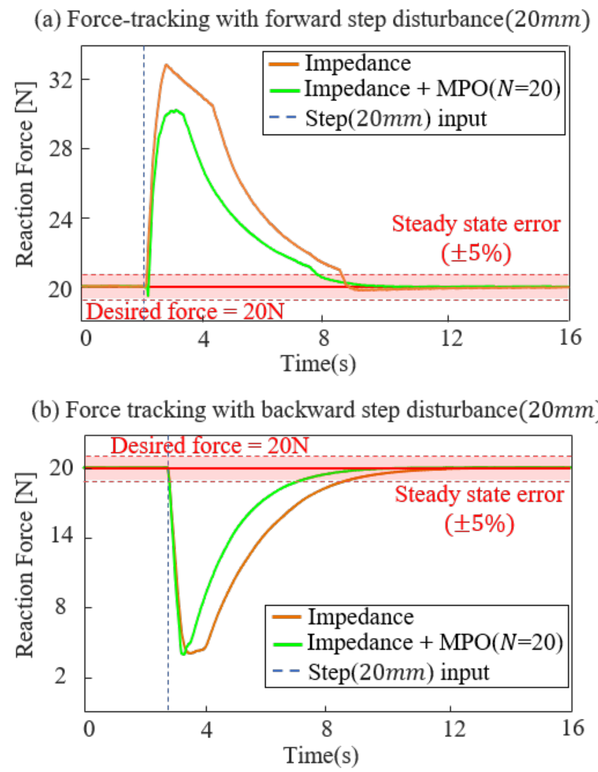

Fig. 12. Force-tracking performance with step(20mm) disturbance. (a) Force-tracking performance with forward step disturbance. (b) Force-tracking performance with backward step disturbance.(N is number of prediction loops)

when N was 20 without grinding, and at the 335th input when N was 30. However, taking into account the actual time required by multiplying the sampling time, it took longer with N=20 at 3.55s and N=30 at 3.69s. In situations where grinding was performed, there was negligible difference between N=20 and N=30 due to the influence of disturbances. Therefore, although optimization performance is superior when N=30, considering the impact of sampling time under the current hardware settings, N=20 was selected as the optimal number of loops. When the number of loops N is 20, it is faster than 1.56s when impedance control is applied alone, resulting in an improvement of 30.5%. Fig. 10 (b) is the result of an experiment to find out the force tracking performance along with the actual grinding work. The overall trend is similar to that of the absence of a grinding operation, but the application of MPO was faster than the existing impedance in the time to reach the steady state for 5% error. The overall tendency is similar to when there is no grinding work. The settling time which enters the steady state for a 5% error is 1.48s faster when the number of loops is 20, and an improvement of 28.1%. The changes in the main values of the controller while the impedance controller to which MPO is applied follows the force after contact with the wall are confirmed through Fig. 11. Looking at the impedance coefficient K_d value in Fig. 11 (a), the higher the number of loops, the faster it decreases and consequently converges at lower values. At the beginning of the control, the value of K_d changes rapidly and K_d value exceeding K_d^{max} is calculated. Thus there is a time when the value of K_d is fixed to K_d^{max} for a predetermined time. This has a slight effect on the convergence speed of the control, but prevents the saturation of the motor, enabling stable behavior overall. Fig. 11 (b) shows the position control input calculated due to the update of K_d. The compliance position x_c predicted through the MPO, the higher the number of prediction loops, the higher the compliance distance. In Eq. (18) expression corresponding to the control algorithm, K_d values and x_c values have an inversely proportional relationship with each other, resulting in a faster lower K_d value and convergence to lower values in the higher number of loops that export higher x_c.

As a result, if the number of predictive loops is as high as Fig. 11 (c) according to the change in the K_d value, the desired distance x_d value is exported, which causes the manipulator to reach the desired force faster.

In order to confirm the force-tracking performance against disturbance of the controller, a comparison was made between the existing controller and the controller applying MPO by giving strong disturbance during force-tracking. The disturbance is a step signal of 20mm and is given in the y-axis direction through the disturbance generator of the test bench of Fig. 9. The result of the controller's force-tracking performance against disturbance is shown in Fig. 12. Fig. 12 (a) shows reaction force when a forward disturbance of 20mm occurs while tracking a desired force of 20N. The reaction force overshoot value due to disturbance of impedance control applied with MPO is 30.1N is 4.34N lower than the existing controller value of 34.44N and the time to return to steady state is also 15.54s, which is a reduction of 0.82s from the existing controller. Fig. 12 (b) shows a situation in which a disturbance of 20 mm is given to the backward in contact with the grinding target. The reaction force was instantaneously lowered by separation from the grinding target, resulting in a 1.75s improvement in the case of controllers applying MPO at the time of returning to normal for the desired force. As a result, it shows that the proposed control method can improve the efficiency of the grinding operation by quickly following the reaction force required for grinding even when a disturbance is applied compared to the existing adaptive impedance controller.

V. Conclusion

There is a limit to controlling the force with general impedance control, because there are many disturbances that are generated when contacting the object during grinding work. Based on the fact that the MPC optimization method calculated through model prediction is effective in a nonlinear environment, an attempt was made to overcome the limitations of impedance control during grinding. Model prediction allows for stronger control in real time by inserting an optimization loop for the impedance coefficient K_d. Experiments were conducted using a prototype robot and a test bench to verify the performance of the model prediction impedance control, which is the proposed control system. The proposed impedance control with MPO showed 28.1% improved setting time for desired force compared to the existing controller, and more robust results for disturbance. The results show that the application of MPO to the impedance improved control performance and gave robustness against disturbance. As a result, impedance control via model-based prediction optimize(MPO)is proposed as a more effective control method for robots used in disturbance-laden grinding tasks.

References

[1] Y. Wang and C. Wang, "Development of a polishing robot system," in *1999 7th IEEE International Conference on Emerging Technologies and Factory Automation. Proceedings ETFA '99 (Cat. No.99TH8467)*, vol. 2, 1999, pp. 1161–1166 vol.2.

[2] M. Ariefiani, L. Handoko, H. N. Amrullah, L. Ashari, M. Shah, and F. Hamzah, "Human error probability of grinding operation in fabrication and construction company using fuzzy heart method," in *Proceedings of the 2019 1st International Conference on Engineering and Management in Industrial System (ICOEMIS 2019)*. Atlantis Press, 2019/11, pp. 118–125. [Online]. Available: https://doi.org/10.2991/icoemis-19.2019.17

[3] H. Zhou, S. Ma, G. L. Wang, Y. Deng, and Z. Liu, "A hybrid control strategy for grinding and polishing robot based on adaptive impedance control," *Advances in Mechanical Engineering*, vol. 13, 2021.

[4] A. Kelm, R. Boerret, and S. Sinzinger, "Improving the polishing accuracy by determining the variance of the friction coefficient," *Journal of the European Optical Society - Rapid publications*, vol. 7, no. 0, 2012.

[5] A. I. Yilmaz, F. Yilmaz, and U. B. Celebi, "Analysis of shipyard accidents in turkey," *British Journal of Applied Science & Technology*, vol. 5, no. 5, p. 472, 2015.

[6] S. Lakshminarayanan, S. Kana, D. M. Mohan, O. M. Manyar, D. J. H. Then, and D. Campolo, "An adaptive framework for robotic polishing based on impedance control," *The International Journal of Advanced Manufacturing Technology*, vol. 112, pp. 401–417, 2020.

[7] M. Jinno, F. Ozaki, T. Yoshimi, K. Tatsuno, M. Takahashi, M. Kanda, Y. Tamada, and S. Nagataki, "Development of a force controlled robot for grinding, chamfering and polishing," in *Proceedings of 1995 IEEE International Conference on Robotics and Automation*, vol. 2, 1995, pp. 1455–1460 vol.2.

[8] L. Kong, W. He, Z. Liu, X. Yu, and C. Silvestre, "Adaptive tracking control with global performance for output-constrained mimo nonlinear systems," *IEEE Transactions on Automatic Control*, 2022.

[9] N. Hogan, "Impedance control: An approach to manipulation," in *1984 American Control Conference*, 1984, pp. 304–313.

[10] T. Kim, S. Yoo, H. S. Kim, and T. Seo, "Position-based impedance control of a 2-dof compliant manipulator for a facade cleaning operation," in *2020 IEEE International Conference on Robotics and Automation (ICRA)*, 2020, pp. 5765–5770.

[11] S. Jung, T. Hsia, and R. Bonitz, "Force tracking impedance control of robot manipulators under unknown environment," *IEEE Transactions on Control Systems Technology*, vol. 12, no. 3, pp. 474–483, 2004.

[12] T. Kim and H. Kim, "Position-based impedance control for force tracking of a wall-cleaning unit," *International Journal of Precision Engineering and Manufacturing*, vol. 17, pp. 323–329, 03 2016.

[13] C. Ott, R. Mukherjee, and Y. Nakamura, "Unified impedance and admittance control," in *2010 IEEE International Conference on Robotics and Automation*, 2010, pp. 554–561.

[14] H. Seraji, "Adaptive admittance control: an approach to explicit force control in compliant motion," in *Proceedings of the 1994 IEEE International Conference on Robotics and Automation*, 1994, pp. 2705–2712 vol.4.

[15] F. Augugliaro and R. D'Andrea, "Admittance control for physical human-quadrocopter interaction," in *2013 European Control Conference (ECC)*, 2013, pp. 1805–1810.

[16] K. P. Tee, R. Yan, and H. Li, "Adaptive admittance control of a robot manipulator under task space constraint," in *2010 IEEE International Conference on Robotics and Automation*, 2010, pp. 5181–5186.

[17] S. Jung and T. Hsia, "Adaptive force tracking impedance control of robot for cutting nonhomogeneous workpiece," in *Proceedings 1999 IEEE International Conference on Robotics and Automation (Cat. No.99CH36288C)*, vol. 3, 1999, pp. 1800–1805 vol.3.

[18] Q. Xu, "Robust impedance control of a compliant microgripper for high-speed position/force regulation," *IEEE Transactions on Industrial Electronics*, vol. 62, no. 2, pp. 1201–1209, 2015.

[19] R. Anderson and M. Spong, "Hybrid impedance control of robotic manipulators," *IEEE Journal on Robotics and Automation*, vol. 4, no. 5, pp. 549–556, 1988.

[20] S. Jung, T. Hsia, and R. Bonitz, "Force tracking impedance control of robot manipulators under unknown environment," *IEEE Transactions on Control Systems Technology*, vol. 12, no. 3, pp. 474–483, 2004.

[21] F. Almeida, A. Lopes, and P. Abreu, "Force-impedance control: a new control strategy of robotic manipulators," *Recent advances in mechatronics*, 01 1999.

[22] R. Carelli and R. Kelly, "An adaptive impedance/force controller for robot manipulators," *IEEE Transactions on Automatic Control*, vol. 36, no. 8, pp. 967–971, 1991.

[23] X. Yu, W. He, Q. Li, Y. Li, and B. Li, "Human-robot co-carrying using visual and force sensing," *IEEE Transactions on Industrial Electronics*, vol. 68, no. 9, pp. 8657–8666, 2020.

[24] C. Yueyan, Z. Ji, W. Bidou, and H. Shuang, "High precision fuzzy impedance control of free-form surfaces polishing robotic arm based on position control," in *Proceedings, 2005 IEEE/ASME International Conference on Advanced Intelligent Mechatronics.*, 2005, pp. 819–824.

[25] M. H. Hamedani, H. Sadeghian, M. Zekri, F. Sheikholeslam, and M. Keshmiri, "Intelligent impedance control using wavelet neural network for dynamic contact force tracking in unknown varying environments," *Control Engineering Practice*, vol. 113, p. 104840, 2021.

[26] Y. Deng, G. Wang, X. Yue, and K. Zhou, "A review of robot grinding and polishing force control mode," in *2022 IEEE International Conference on Mechatronics and Automation (ICMA)*, 2022, pp. 1413–1418.

[27] I. Joo, J. Hong, S. Yoo, J. Kim, H. Kim, and T. Seo, "Parallel 2-dof manipulator for wall-cleaning applications," *Automation in Construction*, vol. 101, pp. 209–217, 05 2019.

[28] H. Chae, G. Park, J. Lee, K. Kim, T. Kim, H. S. Kim, and T. Seo, "Façade cleaning robot with manipulating and sensing devices equipped on a gondola," *IEEE/ASME Transactions on Mechatronics*, vol. 26, no. 4, pp. 1719–1727, 2021.

[29] W. M. dos Santos and A. A. Siqueira, "Optimal impedance via model predictive control for robot-aided rehabilitation," *Control Engineering Practice*, vol. 93, p. 104177, 2019.

[30] W. M. dos Santos and A. A. G. Siqueira, "Optimal impedance control for robot-aided rehabilitation of walking based on estimation of patient behavior," in *2016 6th IEEE International Conference on Biomedical Robotics and Biomechatronics (BioRob)*, 2016, pp. 1023–1028.

ChangKook Seo received his B.S. degree in Mechanical Engineering from Hanyang University in 2021. He is currently working toward his M.S. degree in Mechanical Engineering at Hanyang University. His research interests lie in robot mechanism design.

Hanbom Kim received his B.S. degree in Mechanical Engineering from Hanyang University in 2022. He is currently working toward his M.S. degree in Mechanical Engineering at Hanyang University. His research interests lie in robot mechanism design.

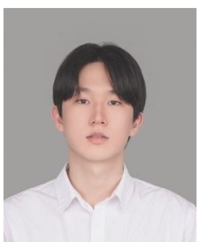

Hongjoo Jin received his B.S. degree in Mechanical Engineering from Hanyang University in 2023. He is currently working toward his M.S. degree in Mechanical Engineering at Hanyang University. His research interests lie in robot mechanism design.

Taegyun Kim received the B.S. and Ph.D. degrees in Mechanical and Aerospace Engineering from Seoul National University, Korea, in 2011 and 2017. He was a Senior Engineer at the Mechatronics R&D Center of SAMSUNG Electronics Company from 2017 to 2019. He is currently an Assistant Professor at the School of Mechanical Engineering, Yeungnam University. His current research interests include robot mechanism design, robust control, and smart factory.

TaeWon Seo (M'10, SM'20) received a B.S. degree and Ph.D. from the School of Mechanical and Aerospace Engineering, Seoul National Univserity, Korea in 2003 and 2008, respectively. He is an Associate Professor at the School of Mechanical Engineering, Hanyang University, Korea. Prior to moving to Hanyang University, he was a postdoctoral researcher at Nanorobotics Laboratory, Carnegie Mellon University, visiting professor at Biomimetic Millisystems Laboratory, UC Berkeley, scholar at the University of Michigan, and associate professor at the School of Mechanical Engineering, Yeungnam University, Korea. His research interests include robot design, analysis, control, optimization, and planning. Dr. Seo received the Best Paper Award from IEEE/ASME Transactions on Mechatronics in 2014. He is a Technical/Associate Editor of IEEE/ASME Transactions on Mechatronics and Intelligent Service Robots, and an Associate Editor of IEEE Robotics and Automation Letters.